Hindawi Publishing Corporation
Journal of Spectroscopy
Volume 2014, Article ID 732163, 6 pages
http://dx.doi.org/10.1155/2014/732163

Research Article

Influence of Zn/Fe Molar Ratio on Optical and Magnetic Properties of ZnO and $ZnFe_2O_4$ Nanocrystal as Calcined Products of Layered Double Hydroxides

Abdullah Ahmed Ali Ahmed,[1] Zainal Abidin Talib,[2] Mohd Zobir Hussein,[3] Moayad Husein Flaifel,[4] and Naif Mohammed Al-Hada[2]

[1] *Department of Physics, Faculty of Applied Science, Thamar University, P.O. Box 87246, Dhamar, Yemen*
[2] *Department of Physics, Faculty of Science, Universiti Putra Malaysia (UPM), 43400 Serdang, Selangor, Malaysia*
[3] *Advanced Materials and Nanotechnology Laboratory, Institute of Advanced Technology (ITMA), Universiti Putra Malaysia (UPM), 43400 Serdang, Selangor, Malaysia*
[4] *School of Applied Physics, Faculty of Science and Technology, Universiti Kebangsaan Malaysia, 43600 Bangi, Selangor, Malaysia*

Correspondence should be addressed to Abdullah Ahmed Ali Ahmed; abdullah2803@gmail.com

Received 25 April 2014; Revised 2 June 2014; Accepted 23 June 2014; Published 10 July 2014

Academic Editor: Jie-Fang Zhu

The coprecipitation method has been used to synthesize layered double hydroxide (Zn-Fe-LDH) nanostructure at different Zn^{2+}/Fe^{3+} molar ratios. The structural properties of samples were studied using powder X-ray diffraction (PXRD). LDH samples were calcined at 600°C to produce mixed oxides (ZnO and $ZnFe_2O_4$). The crystallite size of mixed oxide was found in the nanometer scale (18.1 nm for $ZnFe_2O_4$ and 43.3 nm for ZnO). The photocatalytic activity of the calcination products was investigated using ultraviolet-visible-near infrared (UV-VIS-NIR) diffuse reflectance spectroscopy. The magnetic properties of calcined LDHs were investigated using a vibrating sample magnetometer (VSM). The calcined samples showed a paramagnetic behavior for all Zn^{2+}/Fe^{3+} molar ratios. The effect of molar ratio on magnetic susceptibility of the calcined samples was also studied.

1. Introduction

Layered double hydroxides (LDHs) are one of the popular inorganic hosts to form an organic-inorganic hybrid type nanocomposite or so-called nanolayered composite materials [1]. LDHs, also known as hydrotalcite-like structure and anionic clay compounds, belong to a special class of synthetic two-dimensional inorganic compounds with lamellar structures. The chemical composition of LDHs can be described by the general formula $[M^{2+}_{1-x}M^{3+}_x(OH)_2]^{x+}[(A^{n-})_{xln} \cdot mH_2O]^{x-}$, where M^{2+} = divalent metals, M^{3+} is trivalent metals, and A^{n-} is an anion with charge n. Molar fraction number mol of water in LDH interlayer per formula weight of compounds and $x = M^{3+}/(M^{3+} + M^{2+})$ molar fraction (normally, it is between 0.2 and 0.33) [2].

An important use of LDH precursors is to get mixed nanometal oxides by calcination at temperature above 600°C [3, 4]. This method has been used to address the problem of the fast recombination of photogenerated electron-hole pairs in the mixed semiconductors to enhance the photocatalytic efficiency of semiconductor. Nano-zinc oxide (ZnO) with its excellent features has been used as photocatalysts [5]. At the same time, $ZnFe_2O_4$ spinel, which is a semiconductor with narrow band gap, exhibits characteristics of excellent visible-light response, as well as favorable magnetism and good photochemical stability [6]. In the current paper, Zn-Fe-CO_3-LDH has been synthesized by the coprecipitation method with Zn^{2+}/Fe^{3+} molar ratios of 1, 2, 3, and 4 at the final pH value of 8. The mixed metal oxides were formed by the calcination process of LDH at 600°C. The structural,

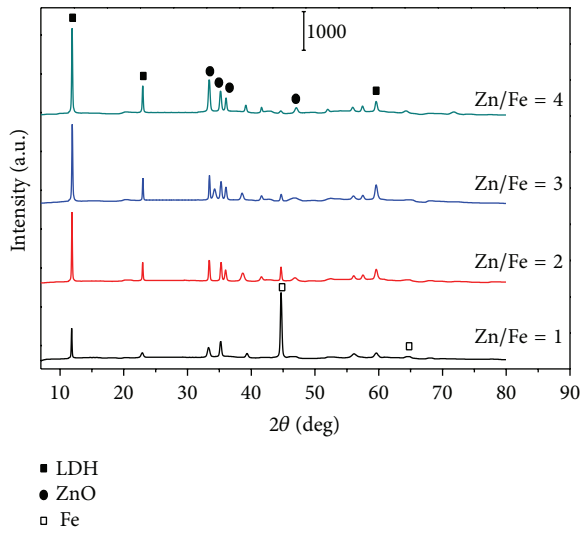

Figure 1: PXRD patterns of Zn-Fe-LDH samples synthesized at different Zn^{2+}/Fe^{3+} molar ratios.

optical, and magnetic properties of calcination products were studied.

2. Experimental

2.1. Synthesis of Zn-Fe-LDH and Its Calcination Products. LDH precursors (Zn-Fe-LDH) were synthesized using coprecipitation method at pH 8 with Zn^{2+}/Fe^{3+} molar ratios of 1, 2, 3, and 4. Zn^{2+}/Fe^{3+} molar ratio was changed to evaluate its effect on the properties of the calcination products of LDH.

The synthesis was carried out by a slow addition of two metal nitrates solutions which were $Zn(NO_3)_2{\cdot}6H_2O$ and $Fe(NO_3)_3{\cdot}9H_2O$. The concentrations of $Zn(NO_3)_2{\cdot}6H_2O$ solution were 0.025, 0.050, 0.075, and 0.1 M for Zn^{2+}/Fe^{3+} molar ratios of 1, 2, 3, and 4, respectively, while the concentration of $Fe(NO_3)_3{\cdot}9H_2O$ solution was fixed at 0.025 M for all samples. The solution that contained 0.1 M of Na_2CO_3 was added slowly (dropwise addition) to the metal nitrates solutions with constant stirring. The pH value for all samples was controlled by addition of aqueous NaOH (0.5 M). The resulting slurry was aged at 70°C for 18 h in an oil bath shaker (50 rpm). The precipitate was washed with deionized water many times with centrifugation. Finally, the precipitate was dried in an oven at 70°C for two days. The resultant Zn-Fe-CO_3-LDH was ground into fine powder.

Heat-treated samples of Zn-Fe-CO_3-LDH were prepared by heating LDH at 600°C. The samples were labeled Z*r*F, where *r* represents the Zn^{2+}/Fe^{3+} molar ratio. Heating was performed in an electric tubular furnace at atmospheric pressure in a ceramic boat holder for 3 h at a rate of 3°C/min (heating and cooling rate). The annealing process was performed in the ambient air. After the heat treatment was completed, the sample was left to cool to room temperature and stored in a sample bottle for further characterization.

2.2. Characterizations. Powder X-ray diffraction (PXRD) patterns of the samples were recorded on an X-ray diffractometer (X'PERT-PRO PANALYTICAL) using CuK_α (λ = 1.54060 Å) at 40 kV and 40 mA. The slit configuration includes the fixing type of the divergence slit with slit size of 0.25°. The goniometer radius is 240 mm and distance of the focus-divergence slit is 100 mm. The scan configuration includes the continuous scan type with step size of 0.0330 [2θ°] and scan step time of 19.685 s. The optical properties were studied using a UV-VIS-NIR diffuse reflectance spectrophotometer (Shimadzu, UV-3600). This spectrophotometer is equipped with an integrating-sphere detector. The magnetic properties of calcined samples were measured using a vibrating sample magnetometer (VSM Model Lakeshore 7404).

3. Results and Discussion

3.1. Powder X-Ray Diffraction (PXRD) Study. Figure 1 shows XRD patterns of Zn-Fe-CO_3-LDH prepared at different Zn^{2+}/Fe^{3+} molar ratios of 1, 2, 3, and 4. XRD patterns exhibit two characteristic intense peaks of basal reflection of Zn-Fe-CO_3-LDH which were located near 2θ of 11.9° and 23.1° corresponding to diffraction by (003) and (006) planes, respectively. As seen in Figure 1, Zn-Fe-CO_3-LDH phase is observed with ZnO phase which was formed during the aging of the coprecipitated products or during the titration process [7, 8]. At Zn^{2+}/Fe^{3+} molar ratio of 1, the Fe metal also was clearly observed. This may be attributed to the presence of a residual of the Fe ions which could not precipitate into prepared Zn-Fe-CO_3-LDH layer. At Zn^{2+}/Fe^{3+} molar ratio values of 2, 3, and 4, the high crystallinity of (003) and (006) peaks was observed which indicated the presence of a well-ordered layered structure [7].

XRD patterns exhibit ZnO/$ZnFe_2O_4$ nanocomposite as the calcination products of Zn-Fe-CO_3-LDH samples at different Zn^{2+}/Fe^{3+} molar ratios (Z1F, Z2F, Z3F, and Z4F) as shown in Figure 2. X'Pert-High-Score Plus software has been used to analyze the XRD data. The peaks of hexagonal wurtzite structure of ZnO were observed near 2θ of 31.8, 34.5, 36.3, 47.7, 56.6, 62.9, 66.5, 68.1, 69.1, and 77° which correspond to diffraction by (100), (002), (101), (102), (110), (103), (200), (112), (201), and (202) planes, respectively, (reference code: 01-079-0206). For $ZnFe_2O_4$ nanocrystal, the peaks were located at 2θ of 18.2, 29.9, 35.2, 42.8, 53.2, 56.6, 62.1, and 66.4° which corresponds to diffraction by (111), (220), (311), (400), (422), (511), (440), and (442) planes, respectively (reference code: 01-089-4926). This is identified as face-centered-cubic (FCC) franklinite $ZnFe_2O_4$ with space group Fd-3m (227) and lattice parameters of $a = b = c = 8.443$ Å.

The crystallinity of ZnO phase increased with the increase in Zn^{2+}/Fe^{3+} molar ratio, while $ZnFe_2O_4$ nanocrystal was observed with almost the same crystallinity due to the fixing of Fe^{3+} content during the preparation of Zn-Fe-CO_3-LDH samples. This observation is in good agreement with the literature [7]. The average crystallite size of $ZnFe_2O_4$ in the (111) crystal plane is 18.1 nm [9] and for ZnO in the (002)

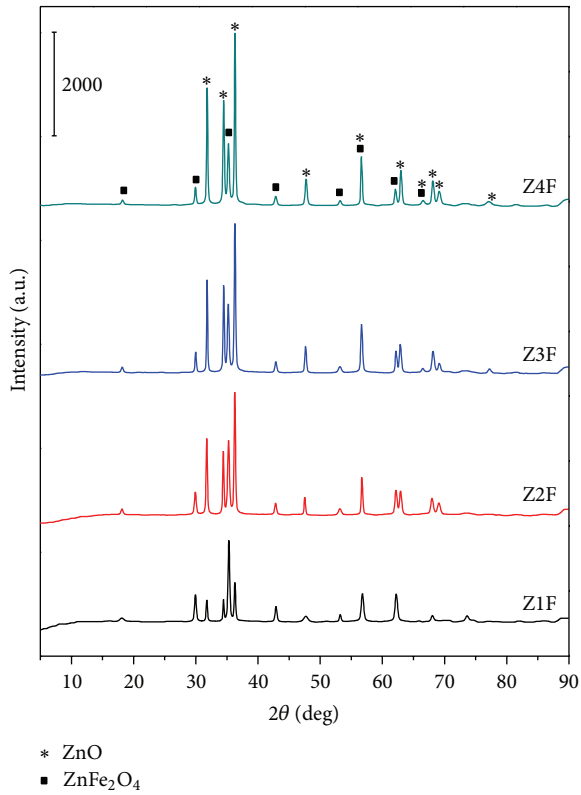

FIGURE 2: PXRD patterns of calcined Zn-Fe-LDH nanostructure.

crystal plane it is 43.3 nm [3, 10, 11] as estimated using Scherrer's equation.

3.2. UV-Visible Spectra. The fundamental absorption of light, which corresponds to an electronic excitation from the valance band to the conduction band, can be applied to calculate the optical band-gap energy (E_g). In this study, the optical band-gap energy can be calculated using the Kubelka-Munk equation in terms of reflectance (R):

$$F(R_\infty) = \frac{(1 - R_\infty)^2}{2R_\infty}, \quad (1)$$

where R_∞ is the diffuse reflectance of the examined samples ($R_\infty = R_{\text{sample}}/R_{\text{standard}}$) and $F(R_\infty)$ is called the remission or Kubelka-Munk function [12, 13]. Thus, the band gap is obtained using the following equation:

$$\left(F(R_\infty) \cdot h\nu\right)^2 = A\left(h\nu - E_g\right). \quad (2)$$

The variation of $(F(R_\infty) \cdot h\nu)^2$ versus $(h\nu)$ is plotted and the straight line range of these plots is extended on $(h\nu)$ axis to obtain the values of optical band gap (E_g).

Figure 3(a) shows the recorded reflectance of calcined Zn-Fe-LDH samples and Figure 3(b) exhibits the band-gap energies of ZnO phase which is found at around 3.19 eV. The average band gap of ZnO/$ZnFe_2O_4$ nanocomposite annealed at 600°C is found at ~2.30 eV as shown in Figure 3(c). The band-gap value of pure $ZnFe_2O_4$ is 1.9 eV [14], while the band gap for whole nanocomposite (ZnO/$ZnFe_2O_4$) increased to 2.32 eV as seen in the recent study [15]. This is in good agreement with our results. On the other hand, the ZnO band-gap energy decreases from ~3.37 eV (for pure ZnO phase) [16] to around 3.19 eV in this work. This phenomenon occurs due to the presence of ZnO with another metal oxide ($ZnFe_2O_4$) which indicates the photocatalytic activity [17]. As seen in Figure 3(c), another band gap also is observed at ~2.70 eV which may be attributed to the presence of ZnO/$ZnFe_2O_4$ nanocomposite.

Table 1 exhibits the effect of Zn^{2+}/Fe^{3+} molar ratio on the crystallite size of mixed metal oxide (ZnO and $ZnFe_2O_4$) and ZnO band-gap energy. As Zn^{2+}/Fe^{3+} molar ratio value increases from 1 to 4, the crystallite size of ZnO phase decreases from 51.2 to 36.6 nm; thus, the ZnO band gap increases from 3.188 to 3.198 eV. The fluctuation in band-gap value of ZnO in Table 1 may be attributed to the additional ZnO phase which formed during the preparation of Zn-Fe-LDH as shown in Figure 1.

As seen in Figure 3(d), the absorbance of LDH calcination products has shown an edge at 360 nm which indicates the free exciton absorption of the lower particle size of ZnO [18]. The broad band at around 295 nm may suggest charge transfer transition from O^{2-} to Fe^{3+} in $ZnFe_2O_4$ spinel [19]. The threshold of the absorption band of $ZnFe_2O_4$ spinel occurs at around 685 nm. The blue shift absorption of $ZnFe_2O_4$ spinel and ZnO compared with the $ZnFe_2O_4$ (700 nm) may be attributed to the quantum-size effect.

Under visible-light irradiation, photogenerated electrons (e) and holes (h) are produced in mixed oxides (ZnO and $ZnFe_2O_4$) via electron excitation from valence band (VB) to conductance band (CB) of $ZnFe_2O_4$ nanocrystal. Due to the differences in the positions of band gap in these oxides, the photogenerated electrons transferred from CB of $ZnFe_2O_4$ to CB of ZnO as illustrated schematically in Figure 4. At the same time, the number of holes with positive charge left (VB) of $ZnAl_2O_4$ to (VB) of ZnO. The difference in the energy levels of ZnO and $ZnFe_2O_4$ semiconductors is important in achieving such charge separation which gives rise to the improvement of the photocatalytic activity of ZnO [17].

3.3. Magnetic Spectroscopy. The magnetic behavior of mixed oxides (ZnO and $ZnFe_2O_4$) as a function of Zn^{2+}/Fe^{3+} molar ratio incorporated is quite different. All calcined samples exhibit a paramagnetic behavior as shown in Figure 5. The typical curves for paramagnetic systems can be defined as

$$M = \chi \cdot H, \quad (3)$$

where M is the magnetization, H is the applied magnetic field, and χ is the magnetic susceptibility.

Normally, the magnetic contribution of pure $ZnFe_2O_4$ nanocrystal below a critical value of particle size 10 nm for [9] is superparamagnetic behavior, while this behavior changed to paramagnetic when $ZnFe_2O_4$ nanocrystal was calcined at temperature of 650°C [9]. This is due to the oxygen vacancies of $ZnFe_2O_4$ fully occupied during the heat treatment in air, which is responsible for the reduction in magnetic moment. In this study, the room temperature magnetic hysteresis loop of the calcined products of LDH (ZnO and $ZnFe_2O_4$) shows

Table 1: Crystallite size and optical band-gap energy (E_g) for Z1F, Z2F, Z3F and Z4F samples.

Samples	ZnO size[a] (nm)	$ZnFe_2O_4$ size[a] (nm)	E_g of ZnO phase (eV)
Z1F	51.2	10.3	3.188 ± 0.014
Z2F	42.7	20.6	3.196 ± 0.015
Z3F	42.7	20.6	3.187 ± 0.020
Z4F	36.6	20.7	3.198 ± 0.018

[a]Crystallite size: calculated using Scherrer's equation.

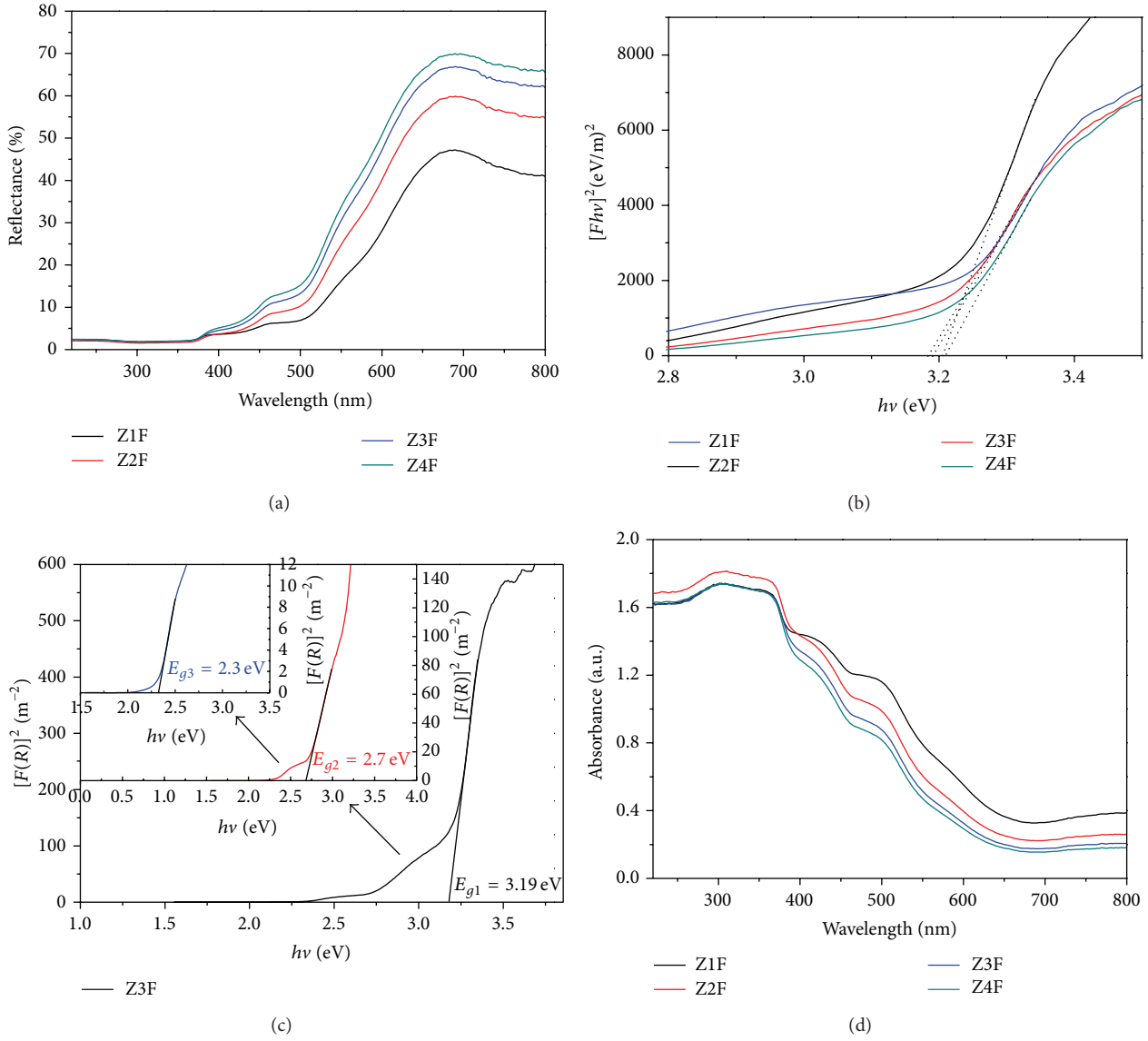

Figure 3: Kubelka-Munk transformed reflectance spectra of (a) reflectance spectra of $ZnO/ZnFe_2O_4$ nanocomposite, (b) band-gap energy of ZnO, (c) Kubelka-Munk plot $ZnO/ZnFe_2O_4$ nanocomposite (for sample Z3F as an example), and (d) diffuse reflectance UV-visible absorption spectra of calcined Zn-Fe-LDH nanostructure.

a paramagnetic behavior as shown in Figure 5. The final magnetization value (there is no saturation magnetization) decreases as Zn content (Zn^{2+}/Fe^{3+} molar ratio) increases due to the presence of high crystalline ZnO. Figure 6 shows the magnetic susceptibility as function of the Zn^{2+}/Fe^{3+} molar ratio in the samples. The value of paramagnetic response (χ) decreases with the increase in Zn^{2+}/Fe^{3+} molar ratio according to the observed formation of ZnO [7].

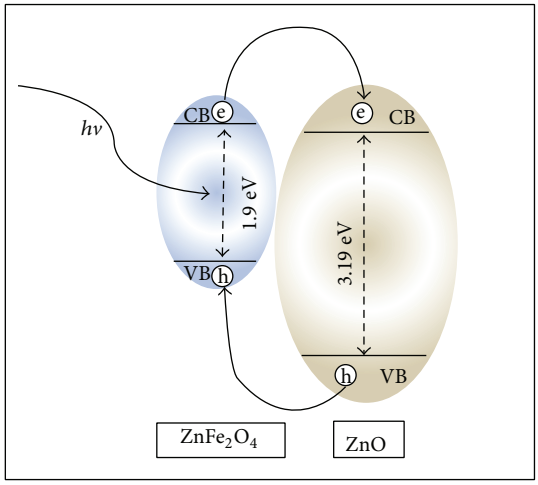

Figure 4: Scheme of the coupling action of different energy bands between ZnO and $ZnFe_2O_4$ [17].

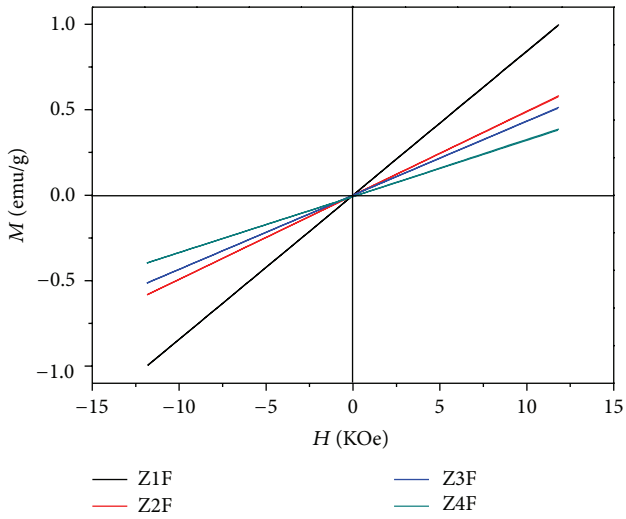

Figure 5: Paramagnetic contribution of the hysteresis loop after the calcination.

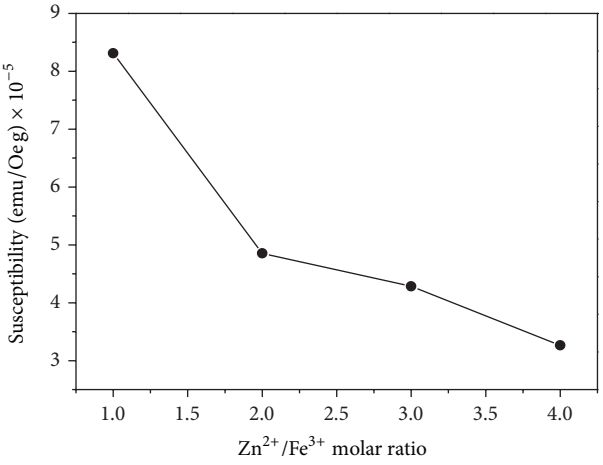

Figure 6: Susceptibility as function of Zn^{2+}/Fe^{3+} molar ratio for calcined samples.

4. Conclusions

The coprecipitation method was used to synthesize Zn-Fe-LDH at the Zn^{2+}/Fe^{3+} molar ratios of 1, 2, 3, and 4. XRD patterns of the calcined LDH showed ZnO and $ZnFe_2O_4$ phases. XRD confirmed that $ZnFe_2O_4$ is composed of franklinite. The crystallite sizes of both phases in nanocrystal range were found as 18.1 nm for $ZnFe_2O_4$ and 43.3 nm for ZnO. The optical band-gap value of ZnO was improved to around 3.19 eV due to the photocatalytic activity, while the optical band-gap energy of $ZnO/ZnFe_2O_4$ nanocomposite was found at around two values of 2.30 and 2.70 eV. The magnetic behavior of mixed oxides (ZnO and $ZnFe_2O_4$) phases showed a paramagnetic behavior due to the oxygen vacancies of $ZnFe_2O_4$ fully occupied during the heat treatment in air, which resulted in the reduction in magnetic moment. The magnetic susceptibility decreased as Zn^{2+}/Fe^{3+} molar ratio increased due to the increase in the crystallinity of formed ZnO.

Conflict of Interests

The authors declare that there is no conflict of interests regarding the publication of this paper.

Acknowledgments

The authors would like to thank Universiti Putra Malaysia (UPM) for supporting this work. A. A. A. Ahmed thanks RMC-UPM for the support.

References

[1] F. Kovanda, E. Jindová, K. Lang, P. Kubát, and Z. Sedláková, "Preparation of layered double hydroxides intercalated with organic anions and their application in LDH/poly (butyl methacrylate) nanocomposites," *Applied Clay Science*, vol. 48, no. 1, pp. 260–270, 2010.

[2] F. Cavani, F. Trifirò, and A. Vaccari, "Hydrotalcite-type anionic clays: preparation, properties and applications," *Catalysis Today*, vol. 11, no. 2, pp. 173–301, 1991.

[3] A. A. A. Ahmed, Z. A. Talib, M. Z. B. Hussein, and A. Zakaria, "Improvement of the crystallinity and photocatalytic property of zinc oxide as calcination product of ZnAl layered double hydroxide," *Journal of Alloys and Compounds*, vol. 539, pp. 154–160, 2012.

[4] M.-Y. Guan, D.-M. Xu, Y.-F. Song, and Y. Guo, "$ZnO/ZnAl_2O_4$ prepared by calcination of ZnAl layered double hydroxides for ethanol sensing," *Sensors and Actuators B: Chemical*, vol. 188, pp. 1148–1154, 2013.

[5] L. Xu, Y.-L. Hu, C. Pelligra et al., "ZnO with different morphologies synthesized by solvothermal methods for enhanced photocatalytic activity," *Chemistry of Materials*, vol. 21, no. 13, pp. 2875–2885, 2009.

[6] X. Li, Y. Hou, Q. Zhao, W. Teng, X. Hu, and G. Chen, "Capability of novel $ZnFe_2O_4$ nanotube arrays for visible-light induced degradation of 4-chlorophenol," *Chemosphere*, vol. 82, no. 4, pp. 581–586, 2011.

[7] A. l. C. Heredia, M. I. Oliva, C. I. Zandalazini et al., "Synthesis, characterization, and catalytic behavior of MgAlZnFe mixed

oxides from precursors layered double hydroxide," *Industrial & Engineering Chemistry Research*, vol. 50, no. 11, pp. 6695–6703, 2011.

[8] A. A. A. Ahmed, Z. A. Talib, and M. Z. bin Hussein, "Thermal, optical and dielectric properties of Zn-Al layered double hydroxide," *Applied Clay Science*, vol. 56, pp. 68–76, 2012.

[9] Y. Sun, W. Wang, L. Zhang, S. Sun, and E. Gao, "Magnetic $ZnFe_2O_4$ octahedra: Synthesis and visible light induced photocatalytic activities," *Materials Letters*, vol. 98, pp. 124–127, 2013.

[10] E. M. Seftel, E. Popovici, M. Mertens et al., "Zn-Al layered double hydroxides: synthesis, characterization and photocatalytic application," *Microporous and Mesoporous Materials*, vol. 113, no. 1–3, pp. 296–304, 2008.

[11] S. Yuan, Y. Li, Q. Zhang, and H. Wang, "ZnO nanorods decorated calcined Mg-Al layered double hydroxides as photocatalysts with a high adsorptive capacity," *Colloids and Surfaces A: Physicochemical and Engineering Aspects*, vol. 348, no. 1–3, pp. 76–81, 2009.

[12] J. Torrent and V. Barron, *Encyclopedia of Surface and Colloid Science*, Marcel Dekker, New York, NY, USA, 2002.

[13] P. F. Wang, Z. H. Li, and Y. M. Zhu, "Research on the direct doping effect of silicon on cubic boron nitride ceramics by UV-VIS diffuse reflectance," *Materials Chemistry and Physics*, vol. 123, no. 2-3, pp. 356–359, 2010.

[14] J. S. Jang, P. H. Borse, J. S. Lee et al., "Synthesis of nanocrystalline $ZnFe_2O_4$ by polymerized complex method for its visible light photocatalytic application: an efficient photo-oxidant," *Bulletin of the Korean Chemical Society*, vol. 30, pp. 1738–1742, 2009.

[15] M. H. Habibi and A. H. Habibi, "Nanostructure composite $ZnFe_2O_4FeFe_2O_4ZnO$ immobilized on glass: photocatalytic activity for degradation of an azo textile dye F3B," *Journal of Industrial and Engineering Chemistry*, vol. 20, no. 1, pp. 68–73, 2013.

[16] Z. L. Wang, "Zinc oxide nanostructures: growth, properties and applications," *Journal of Physics: Condensed Matter*, vol. 16, pp. R829–R858, 2004.

[17] L. Sun, R. Shao, L. Tang, and Z. Chen, "Synthesis of $ZnFe_2O_4$/ZnO nanocomposites immobilized on graphene with enhanced photocatalytic activity under solar light irradiation," *Journal of Alloys and Compounds*, vol. 564, pp. 55–62, 2013.

[18] D. Sridev and K. Rajendran, "Synthesis and optical characteristics of ZnO nanocrystals," *Bulletin of Materials Science*, vol. 32, no. 2, pp. 165–168, 2009.

[19] T. Xie, L. Xu, C. Liu, and Y. Wang, "Magnetic composite $ZnFe_2O_4/SrFe_{12}O_{19}$: preparation, characterization, and photocatalytic activity under visible light," *Applied Surface Science*, vol. 273, pp. 684–691, 2013.